Computers & Geosciences 35 (2009) 255–266

Contents lists available at ScienceDirect

Computers & Geosciences

journal homepage: www.elsevier.com/locate/cageo

CR1Dinv: A Matlab program to invert 1D spectral induced polarization data for the Cole–Cole model including electromagnetic effects ☆

Ahmad Ghorbani [a,*], Christian Camerlynck [a], Nicolas Florsch [b]

[a] UMR 7619 "Sisyphe", Université Pierre et Marie Curie, Paris, France
[b] UMMISCO/IRD, UPMC/Paris and Department of Mathematics and Applied Mathematics, Cape Town University, South Africa

ARTICLE INFO

Article history:
Received 2 February 2007
Received in revised form
12 June 2008
Accepted 23 June 2008

Keywords:
Complex resistivity
Cole–Cole model
Spectral induced polarization
EM coupling
Homotopy inversion method

ABSTRACT

An inversion code has been constructed using Matlab, to recover 1D parameters of the Cole–Cole model from spectral induced polarization data. In a spectral induced polarization survey, impedances are recorded at various frequencies. Both induced polarization and electromagnetic coupling effects occur simultaneously over the experimental frequency bandwidth, and these become progressively more dominant when the frequency increases. We used the CR1Dmod code published by Ingeman-Nielsen and Baumgartner [2006]. This code solves for electromagnetic responses, in the presence of complex resistivity effects in a 1D Earth. In this paper, a homotopy method has been designed by the authors to overcome the local convergence problem of normal iterative methods. In addition, in order to further condition the inverse problem, we incorporated standard Gauss–Newton (or quasi-Newton) methods. Graphical user interfaces enable straightforward entering of the data and the *a priori* model, as well as the cable configuration. Two synthetic examples are presented, showing that the spectral parameters can be recovered from multifrequency, complex resistivity data.

1. Introduction

Spectral induced polarization (SIP) is widely used in environmental and engineering geophysical prospecting, as well as in mineral exploration (e.g., Pelton et al., 1978; Luo and Zhang, 1998), in hydrogeophysics (e.g., Klein and Sill, 1982; Kemna, 2000; Kemna et al., 1999, 2004; Binley et al., 2005), and in the study of organic and non-organic contamination of soils and rocks (e.g., Vanhala, 1997; Abdel Aal et al., 2006).

The mutual impedances of grounded wires (electromagnetic coupling between the transmitter, the receiver and the ground) are of prime importance in SIP surveys. At low frequencies, the electromagnetic (EM) coupling and normal polarization effects of the subsurface material have a similar functional behaviour to the Earth's conductivity, and their combined effects are recorded in a SIP survey. EM coupling is a major impediment in the interpretation of induced polarization (IP) data, and is also known to increase with dipole length and separation, and with conductivity and frequency (Millett, 1967; Dey and Morrison, 1973; Hohmann, 1973; Wait and Gruszka, 1986). For deep exploration, the dipoles and their separation must be large, and the operational frequency is thus usually low in order to avoid EM coupling effects. Unfortunately, the phase angles related to the EM coupling may increase, even at frequencies as low as 1.0 Hz, depending on the ground resistivity, and array type

☆ Code available from server at http://www.iamg.org/CGEditor/index.htm.

* Corresponding author. Tel.: +33 (0) 144274823; fax: +33 (0) 144274588.
E-mail addresses: ghorbani@ipgp.jussieu.fr, ah.ghorbani@yahoo.fr (A. Ghorbani).

0098-3004/$ - see front matter © 2008 Elsevier Ltd. All rights reserved.
doi:10.1016/j.cageo.2008.06.001

and geometry (Gasperikova and Morrison, 2001). One way to avoid EM coupling is to measure SIP data at frequencies low enough for any EM coupling to be either negligible or predictable (Katsube and Collett, 1973; Wynn and Zonge, 1975, 1977). Loke et al. (2006) use a regularized least-squares optimization method to recover the SIP parameters in the 2D problem, but reduced the EM coupling phenomena by limiting the maximum frequency to the range 10–100 Hz. However, the avoidance of high frequencies in the IP spectrum also deprives the user of important information.

Generally, with the time domain IP method, one hopes and expects to avoid the problem of EM coupling by using a "delay time" (i.e., waiting a suitable length of time, in general a few tens of milliseconds) after the transmitter has been switched off, before starting to acquire useful data. During this delay it is assumed that the EM coupling together with time domain transient phenomena will vanish, or reduce to negligible levels. However, the coupling problem cannot be avoided using this approach in highly conductive environments.

In SIP literature, numerous approaches have been proposed, to remove EM coupling effects in SIP data (e.g., Coggon, 1984; Song, 1984; Pelton et al., 1978; Brown, 1985; Cao et al., 2005; Routh and Oldenburg, 2001). However, all of these studies deal with dipole–dipole electrode arrays.

A forward modeling code was developed by Ingeman-Nielsen and Baumgartner (2006), which is capable of handling several commonly used electrical and EM methods in a 1D environment. This code calculates the mutual impedance of 1D ground layers, at different frequencies, for the Cole–Cole model, and different grounded electrode arrays. It also considers the influence of the routing of the wires.

Generally, the generalized inversion method is used to solve the required nonlinear inversion (e.g., Tarantola and Valette, 1982b). If applied to nonlinear equations such as the mutual impedance equation (Sunde, 1968), this method is justified when the initial solution is in the neighbourhood of the global minimum of the objective function. This is a reasonable assumption where good *a priori* knowledge of the field's geology is available. Indeed, the presence of numerous local minima in the objective function prevents iterative optimization techniques from working effectively.

The homotopy method is a powerful tool for solving nonlinear problems, due to its widely convergent properties (Watson, 1989). Homotopy was first used in geophysical applications to solve the seismic ray-tracing problem (Keller and Perozzi, 1983). Vasco (1994, 1998) used homotopy to solve the inverse problem, illustrating its usefulness for travel time tomography and for solving regularized inverse seismic problems. Everett (1996) applied this method to solve the inverse EM problem based on finite difference modeling. Jegen et al. (2001) applied the classic Euler–Newton numerical continuation scheme to the inverse problem, Bao and Liu (2003) constructed a homotopy-regularization method to solve inverse scattering problems with multi-experimental limited aperture data, and Han et al. (2005) used a homotopy method for the inversion of a 2D acoustic wave equation.

The goal of the present paper is to develop the 1D inversion of IP and EM coupling integrals according to the forward modeling code of Ingeman-Nielsen and Baumgartner (2006). A homotopy method is applied to overcome the local convergence shortcomings of Gauss–Newton and quasi-Newton methods.

This paper is organised as follows: firstly, the background of EM coupling theory and forward modeling and inversion process are recalled; then, our program structure is described in detail. Finally, the results obtained with synthetic data, using our inversion code, are presented.

2. Background of EM-coupling theory and forward modeling

In general, for two pairs of grounded electrodes at the Earth's surface, the mutual impedance between the two electrode circuits is defined as the ratio of the voltage in the secondary circuit to the current in the primary circuit:

$$Z(\omega) = E_2(\omega)/I_1(\omega) \tag{1}$$

where I_1 is the alternating current passing through the current electrodes, and E_2 is the electromotive force between the potential electrodes.

This mutual impedance involves a CR contribution, due to the Earth-return currents, and an induced coupling (IC) contribution, due to induction between the wire loops above the ground surface, just as if the loops were not grounded (Brown, 1985). According to Sunde (1968), the EM coupling between two grounded wires in an arbitrary configuration on the surface of the Earth can be calculated by integrating the mutual impedances of a multitude of virtual dipoles along the paths of the wires:

$$\begin{aligned} Z(\omega) &= \int_A^B \int_a^b \left[P(r)\cos\,\xi + \frac{\partial^2 Q(r)}{\partial S \partial s} \right] \mathrm{d}s\,\mathrm{d}S \\ &= \int_A^B \int_a^b P(r)\cos\,\xi\,\mathrm{d}s\,\mathrm{d}S + Q(|Aa|) \\ &\quad + Q(|Ba|) + Q(|Ab|)Q(|Bb|) \end{aligned} \tag{2}$$

where A, B and a, b are the end points of the transmitter and receiver wires (the grounding points), dS and ds are infinitesimal elements of the two wires (the virtual dipoles), ξ the angle between the wire elements, and r the distance between them (Fig. 1). Usually, when dealing with EM coupling, the conductivity is considered to be constant and real, and the permittivity is most often neglected. With these assumptions, applied to a homogeneous half-space, the Q-function is real and constant (frequency independent), and depends only on the position of the grounding points of the wires. It is therefore often referred to as the grounding function. The P-function, although it contains a purely resistive term, is referred to as the coupling function.

One component of the forward modeling algorithm *CR1Dmod* (Ingeman-Nielsen and Baumgartner, 2006) is dedicated to calculating the EM response in the presence of CR effects. This software handles frequency domain

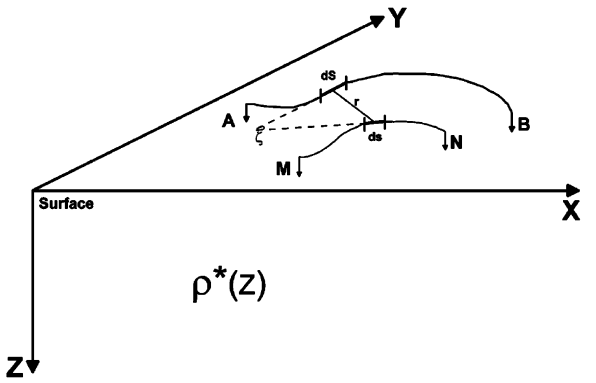

Fig. 1. Earth model and grounded wire, in a common array with two wires on the surface. *A, B* and *a, b* are end points of transmitter and receiver wires, respectively. d*S* and d*s* are infinitesimal elements of two wires, ξ is angle between wire elements and *r* is distance between them. $\rho^*(z)$ indicates the complex resistivity in *Z* direction.

coupling for grounded wires. The wires may be divided into any number of arbitrarily oriented linear segments, provided the receiver and transmitter wires do not intersect.

It is therefore usual practice to calculate a half-space response, analytically based on the properties of the first layer, and add to this a correction term, which accounts for the summed effect of the additional layering. Analytical solutions for the Hankel transforms in the *P*-function of the grounded wire response are computed for non-magnetic homogeneous half-spaces. Calculations can be performed using the full solutions, or the new non-magnetic approximation together with the traditional quasi-static or low-frequency approximation.

3. The Cole–Cole model

Many different models have been proposed for the description of the dispersive behaviour of complex resistivity (Marshall and Madden, 1959; Van Voorhis et al., 1973; Vinegar and Waxman, 1984; Dias, 2000), but the most widely used seems to be the empirical Cole–Cole model, which was originally developed by Cole and Cole (1941) to describe dielectric dispersion. It was shown by Pelton et al. (1978) to accurately describe the resistivity dispersion observed in field data from areas with metallic mineral content. Recent studies have shown that the Cole–Cole parameters can be used to estimate the hydraulic conductivity of sediments (Binley et al., 2005). The Cole–Cole model is given by

$$\rho(\omega) = \rho_0\left(1 - m\left(1 - \frac{1}{1 + (j\omega\tau)^c}\right)\right) \tag{3}$$

where ρ_0 is the resistivity at the DC limit, m the chargeability, τ the time constant, and c the frequency dependence.

These four parameters make the Cole–Cole model sufficiently flexible to adapt itself to a large number of cases. The Cole–Cole resistivity model has been implemented in forward modeling (Ingeman-Nielsen and Baumgartner, 2006), which we have used in the inversion procedure. Whenever modifications are required, one has simply to modify the inversion software with another model, by modifying the *Z_CR .m* code file together with the input and output interface windows.

4. Homotopy inversion theory

Homotopy is a method used to find solutions to general systems of nonlinear equations $\mathbf{L}(\mathbf{P}) = 0$.

A homotopy function $\mathbf{H}(\mathbf{P},\lambda)$ is constructed by adding to the "target function" $\mathbf{L}(\mathbf{P})$ a scalar homotopy parameter λ and a second function $\mathbf{g}(\mathbf{P})$, so that

$$\mathbf{H}(\mathbf{P},\lambda) = \lambda\mathbf{L}(\mathbf{P}) + (1-\lambda)\mathbf{g}(\mathbf{P}) \tag{4}$$

The "initial equation" for the nonlinear equations $\mathbf{g}(\mathbf{P}) = 0$ can be chosen arbitrarily, the only restriction being that it must possess at least one known solution, denoted $\mathbf{P} = \mathbf{A}$.

For the initial value $\lambda = 0$, the homotopy function $\mathbf{H}(\mathbf{P},\lambda)$ has a solution at $\mathbf{A}$, since $\mathbf{H}(\mathbf{A},\lambda) = \mathbf{g}(\mathbf{A}) = 0$. With the aid of numerical continuation methods, starting from the known point $\mathbf{A}$ and $\lambda = 0$, a trajectory is mapped out in $(\mathbf{P},\lambda)$ space such that the homotopy function $\mathbf{H}(\mathbf{P},\lambda)$ vanishes.

A solution $\mathbf{P}^*$ for the target equation $\mathbf{L}(\mathbf{P}) = 0$ occurs at any point where $\mathbf{H}(\mathbf{P},\lambda) = 0$ intersects $\lambda = 1$, since at these locations $\mathbf{H}(\mathbf{P}^*,1) = \mathbf{L}(\mathbf{P}^*) = 0$. The advantageous application of homotopy methods to geophysics can be readily appreciated, if a geophysical inverse problem is formulated as a nonlinear equation of the type $\mathbf{L}(\mathbf{P}) = 0$, since all solutions $\mathbf{P}^*$ found by the homotopy path-tracking algorithm, which satisfy $\mathbf{L}(\mathbf{P}^*) = 0$, are solutions of the inverse problem (Jegen et al., 2001).

5. Generalized nonlinear inverse problem

The knowledge of the probability law for each parameter, has been written by Tarantola and Valette (1982a) as

$$\sigma_{\mathbf{p}}(\mathbf{p}) = \rho_{\mathbf{p}}(\mathbf{p}) \cdot \frac{\rho_{\mathbf{d}}(\mathbf{g}(\mathbf{p}))}{\mu_{\mathbf{d}}(\mathbf{g}(\mathbf{p}))} \tag{5}$$

where $\sigma_{\mathbf{p}}(\mathbf{p})$ is the *a posteriori* probability density for the parameter vector $\mathbf{p}$, $\rho_{\mathbf{p}}(\mathbf{p})$ is the *a priori* probability density, $\rho_{\mathbf{d}}(\mathbf{g}(\mathbf{p}))$ is the probability density of the model for parameter vector $\mathbf{p}$ and data $\mathbf{d}$, and $\mu_{\mathbf{d}}(\mathbf{g}(\mathbf{p}))$ corresponds to null information (full ignorance or homogeneous probability density (HPD)) concerning the parameter. $\mathbf{g}(\mathbf{p})$ is the theoretical relationship between parameter vector $\mathbf{p}$ and data $\mathbf{d}$ which may be considered to be exact.

This equation solves the inverse problem for an exact non-linear model, with an arbitrary *a priori* constraint on parameters ($\rho_{\mathbf{p}}$), and an arbitrary probabilistic data distribution ($\rho_{\mathbf{d}}$).

For quasi-linear problems, if the relationship linking the observable data $\mathbf{d}$ to the model parameters $\mathbf{p}$, $\mathbf{d} = \mathbf{g}(\mathbf{p})$, is approximately linear inside the domain of significant *a priori* probability, then the *a posteriori* distribution is just

as simple as the *a priori* distribution. For instance, an *a priori* Gaussian distribution obviously leads to an *a posteriori* Gaussian distribution. In this case also, the problem can be simplified to the computation of the mean and covariance of the Gaussian distribution. It is supposed hereafter, that the *a priori* information has a Gaussian form.

If the probability distributions are 'bell-shaped' (i.e., if they look like Gaussians, or generalized Gaussians), then one can simplify the problem by calculating the solution only for the point around which the probability is maximum, using an approximate estimation covariance matrix.

If the probability densities are assumed to be Gaussian:

$$\rho_{\mathbf{p}}(\mathbf{p}) = const.\exp\left(-\frac{1}{2}(\mathbf{p}-\mathbf{p}_{prior})^T\mathbf{C}_{\mathbf{p}}^{-1}(\mathbf{p}-\mathbf{p}_{prior})\right) \quad (6)$$

$$\rho_{\mathbf{d}}(\mathbf{d}) = const.\exp\left(-\frac{1}{2}(\mathbf{d}-\mathbf{d}_{obs})^T\mathbf{C}_{\mathbf{d}}^{-1}(\mathbf{d}-\mathbf{d}_{obs})\right) \quad (7)$$

where $\mathbf{C_p}$ and $\mathbf{C_d}$ are covariance matrix parameters and data, respectively. If we assume the nonlinearities to be weak we obtain the following *least squares misfit* function:

$$S(\mathbf{p}) = (\mathbf{p}-\mathbf{p}_{prior})^T\mathbf{C}_{\mathbf{p}}^{-1}(\mathbf{p}-\mathbf{p}_{prior}) + (\mathbf{g}(\mathbf{p})-\mathbf{d}_{obs})^T\mathbf{C}_{\mathbf{d}}^{-1}(\mathbf{g}(\mathbf{p})-\mathbf{d}_{obs}) \quad (8)$$

We apply the steepest descent algorithm (Gauss–Newton method) in order to minimize the $S(\mathbf{p})$ function. If one considers the gradient $\gamma_\alpha = (\partial S)/(\partial \mathbf{p}^\alpha)$, the Gauss–Newton algorithm is an iterative algorithm passing from point $\mathbf{p}_k$ to point $\mathbf{p}_{k+1}$, by means of the following expression (Mosegaard and Tarantola, 2002):

$$\mathbf{p}_{k+1} = \mathbf{p}_k - \varepsilon_k(\mathbf{G}_k^T\mathbf{C}_{\mathbf{d}_0\mathbf{d}_0}^{-1}\mathbf{G}_k + \mathbf{C}_{\mathbf{p}_0\mathbf{p}_0}^{-1})^{-1} \times [\mathbf{G}_k^T\mathbf{C}_{\mathbf{d}_0\mathbf{d}_0}^{-1}(\mathbf{g}(\mathbf{p}_k)-\mathbf{d}_{obs}) + \mathbf{C}_{\mathbf{p}_0\mathbf{p}_0}^{-1}(\mathbf{p}_k-\mathbf{p}_{prior})] \quad (9)$$

where $\mathbf{p}_{prior}$ is the initial estimation for the parameter vector $\mathbf{p}$, $\mathbf{p}_k$ its estimated value at iteration step k, $\mathbf{C}_{\mathbf{p}_0\mathbf{p}_0}$ the parameter covariance matrix (often diagonal because poorly known), $\mathbf{C}_{\mathbf{d}_0\mathbf{d}_0}$ the data covariance matrix (also diagonal because the data are independent), $\mathbf{G}_k$ and $\mathbf{G}_k{}^T$ the matrix corresponding to the derivative of the data with respect to the parameters, and its transpose, $\mathbf{d}_{obs}$ the data vector, and ε_k an *ad hoc* (real, positive) value adjusted to force the algorithm to converge rapidly (if ε_k is chosen to be too small, convergence may be too slow; if it is chosen to be too large, the algorithm may even diverge).

With the Gauss–Newton least-squares method, the Jacobian matrix is recalculated at each iteration, and these calculations can be the most time-consuming steps of the inversion process. In order to reduce the computing time, Loke and Dahlin (2002) used a quasi-Newton method to estimate the Jacobian-matrix values.

Jacobian-matrix values can be calculated during the first iteration. Then the Jacobian matrix is estimated, during each iteration, using the following update equation:

$$\mathbf{G}_{k+1} = \mathbf{G}_k + \mathbf{u}_k \cdot \Delta\mathbf{p}_k^T \quad (10)$$

where $\Delta\mathbf{p}_k$ is the perturbation vector to the model parameters, $\mathbf{u}_k$ $(\Delta\mathbf{g}_k - \mathbf{G}_k\cdot\Delta\mathbf{p}_k)/\Delta\mathbf{p}_k{}^T\cdot\Delta\mathbf{p}_k$, $\Delta\mathbf{g}_k = \mathbf{g}_{k+1} - \mathbf{g}_k$, and $\mathbf{G}_{k+1}$ is the approximate Jacobian matrix for the $(k+1)$th iteration, $\mathbf{g}_k$ is the model response for the kth iteration, and $\Delta\mathbf{g}_k$ is the change in the model.

In theory, the convergence rate of the quasi-Newton method is slower than that of the Gauss–Newton method. Although the quasi-Newton method could require more iterations than the Gauss–Newton method, to converge, the time taken per iteration can be considerably less. We nevertheless propose both methods in our code.

Hereafter, the following assumptions are made:

- The data, $\mathbf{d}$, has Gaussian distribution.
- The parameters, $\mathbf{p}$, for each horizontal layer, are obtained using the Cole–Cole model. The inversion parameters ρ_{0k}, m_k, c_k, and τ_k are respectively: static resistivity, chargeability, frequency dependence, and relaxation time, with k being the layer index.
- The HPD is constant; this term is non-trivial, and Tarantola and Valette (1982a) proposed to define HPD using a parameter from the parameterization invariance with respect to a group transformation. In our case, the parameters ρ_{0k} and τ_k are positive; therefore, their logarithmic character lead to state that both HPD for $\log(\rho_{0k})$, and $\log(\tau_k)$ ($\mu[\log(\rho_{0k})]$ and $\mu[\log(\tau_k)]$) are constant. Here, for instance, $\mu[\log(\tau_k)]$ describes the null information, or HPD for $\log(\tau_k)$. We also considered $\mu[\log(m/(1-m))]$ and $\mu[\log(c/(1-c))]$ constant. The last relations are explained in detail by Ghorbani et al. (2007).
- There is an explicit relationship $\mathbf{d} = \mathbf{g}(\mathbf{p})$, where $\mathbf{d}$ is the data vector and $\mathbf{p}$ the parameter vector to be solved for; in our case, this is provided by Eq. (2). The relationship $\mathbf{d} = \mathbf{g}(\mathbf{p})$ is assumed to be exact.

6. Inversion process

In this section, the implementation of the continuation (homotopy) inversion process is explained. The input data consists of amplitude and phase data at a number of frequencies, which is converted to real and imaginary resistivity values during the inversion processes. The measurements should be performed at a minimum of four frequencies, spread over a suitably wide range, since a single, simple Cole–Cole model has four parameters. The parameter vector $\mathbf{p}$ finally reduces to $[\hat{\rho}_{0i}, \hat{m}_i, \hat{c}_i, \hat{\tau}_i, \hat{h}_i]^T$. Where $\hat{\rho}_{0i} = \log(\rho_{0i})$, $\hat{m}_i = \log(m_i/(1-m_i))$, $\hat{c}_i = \log(c_i/(1-c_i))$, $\hat{h}_i = \log(h_i)$, and i is the layer index.

The first part of the inversion process involves the determination of an initial 1D resistivity model, based on the apparent DC resistivity values, by means of an approximate inversion. The amplitudes of the apparent-impedance values, measured at the lowest frequency, can be used as DC resistivity values. To invert $\hat{\rho}_{0i}$ and $\hat{h}_i$ in the initial model, m_i is considered to be zero. Therefore, in this case, forward modeling is similar to using a DC resistivity model. The Gauss–Newton method (Eq. (9)) is then used to construct the initial resistivity and thickness model.

The second part of the inversion process consists in implementing the homotopy technique, using Gauss–Newton or quasi-Newton methods to minimize the misfit function in each step.

The parameters obtained in the earlier part of the process are used to compute the starting model for the homotopy inversion. We use a linear combination function of $\mathbf{g}(\mathbf{P})$:

$$\mathbf{h}(\mathbf{P},\lambda) = \lambda \mathbf{d}_{obs} + (1-\lambda)\mathbf{g}_0(\mathbf{P}_0) \quad (11)$$

where $\mathbf{d}_{obs}$ is the vector containing the in-phase and out-of-phase parts of the complex resistivity measurements; $\mathbf{g_0}$ the vector of the real and imaginary resistivities obtained by forward modeling, using the initial parameter vector $\mathbf{p_0}$; $\mathbf{p}$ the parameter vector; and λ a real variable, which ranges between 0 and 1.

Here, it is assumed that the physics-based forward response is capable of predicting the data vector, $\mathbf{d} = \mathbf{g}(\mathbf{p}^*)$. The first value of λ is 0, which increases in subsequent steps. It is clear that $\mathbf{g}(\mathbf{P},\lambda = 0) = \mathbf{g_0}(\mathbf{P_0})$ is the same starting model vector. When λ increases, the other model vectors are estimated, such that the influence of the data measurement vector increases and the influence of the initial model vector decreases. In this study, path-tracking is based on a set of predictor–corrector steps. The predictor step consists in varying the model vector $(\mathbf{P},\lambda)$ by $\Delta\lambda$ along the λ-direction (Benavides and Everett, 2007). We used an isometric division for $\Delta\lambda$, or $\lambda_j = j/N$ where $j = 1, \ldots, N$, as it has been shown to give satisfactory results (Benavides and Everett, 2007; Han et al., 2007). The corrector step is a Gauss–Newton (or quasi-Newton) algorithm, which is used to minimize the misfit function at each step of the homotopy inversion. Once the corrector step has been completed, the next predictor step is initiated. At the jth predictor–corrector step, the predicted model vector is $(\mathbf{p}_k, j.\Delta\lambda)$. Assuming the solution $\mathbf{p}^j$ for the jth equation to have been obtained, the successive Gauss–Newton (or quasi-Newton) method can be used to solve the $(j+1)$th equation. The iteration formula for solving the jth step of the homotopy Eq. (11), taking into account the Gauss–Newton expression (9), is thus given by the following:

$$\mathbf{p}^j_{k+1} = \mathbf{p}^j_k - \varepsilon_k(\mathbf{G}_k^T\mathbf{C}^{-1}_{\mathbf{d}_0\mathbf{d}_0}\mathbf{G}_k + \mathbf{C}^{-1}_{\mathbf{p}_0\mathbf{p}_0})^{-1} \times [\mathbf{G}_k^T\mathbf{C}^{-1}_{\mathbf{d}_0\mathbf{d}_0}(\mathbf{g}(\mathbf{p}_k) - \mathbf{h}(\mathbf{p}_k,\lambda_j)) + \mathbf{C}^{-1}_{\mathbf{p}_0\mathbf{p}_0}(\mathbf{p}_k - \mathbf{p}_{prior})] \quad (12)$$

where k is the iteration index of the Gauss–Newton iterations, and $k = 0, 1, \ldots, k_T$.

Alternatively:

$$\mathbf{p}^j_{k+1} = \mathbf{p}^j_k - \varepsilon_k(\mathbf{G}_k^T\mathbf{C}^{-1}_{\mathbf{d}_0\mathbf{d}_0}\mathbf{G}_k + \mathbf{C}^{-1}_{\mathbf{p}_0\mathbf{p}_0})^{-1} \times \left\{\mathbf{G}_k^T\mathbf{C}^{-1}_{\mathbf{d}_0\mathbf{d}_0}\left[\mathbf{g}(\mathbf{p}_k) - \left(\left(1-\frac{j}{N}\right)\mathbf{g}_0(\mathbf{p}_0) + \frac{j}{N}\mathbf{d}_{obs}\right)\right] + \mathbf{C}^{-1}_{\mathbf{p}_0\mathbf{p}_0}(\mathbf{p}_k - \mathbf{p}_{prior})\right\} \quad (13)$$

The Jacobian-matrix values are obtained from the numerical derivative given by forward modeling. Fig. 2 schematically illustrates the algorithm used during the inversion process.

7. Program structure

CR1Dinv comprises three main windows: the *CR1Dinv* window, the *SondagePoint* window and the *Calculate* window. The *CR1Dinv* window controls the starting parameters, its standard deviation, and the number of sounding data points; the *SondagePoint* window controls the configuration of the sounding points; the *Calculate* window controls the specific parameters and inversion routines used in the calculations. The left-hand side of *CR1Dinv* window features an interactive plot of the half-space model (Fig. 3). By mouse clicking on the plot, the user can insert layer boundaries and drag them to the desired position. On the right-hand side of the same window, the lower section contains input fields for the *a priori* layer parameters, including the *a priori* Cole–Cole model parameters and their standard deviation, relative permittivity $(\varepsilon_r = \varepsilon/\varepsilon_0)$ and magnetic susceptibility $(\chi = \mu/\mu_0 - 1)$. It also enables layers to be added or deleted from the model. The upper right-hand section of this window provides for control of the measurement configurations. A dipole–dipole array or a general surface array (GSA) can be selected. The GSA allows for arbitrary location of the receiver and transmitter electrodes on the surface of the layered half-space.

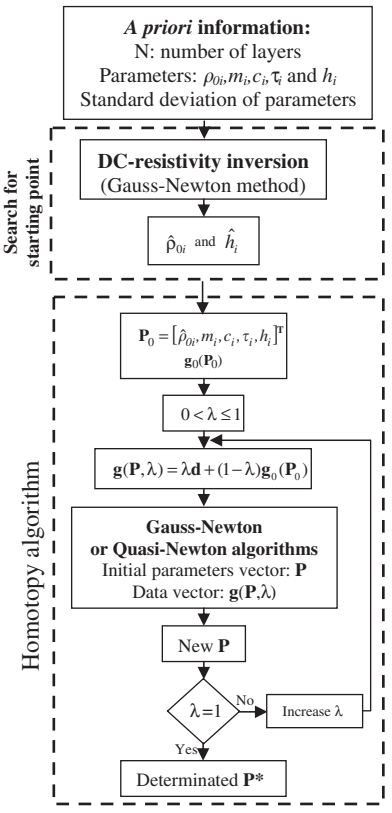

Fig. 2. Simplified illustration of inversion algorithm.

Before entering the data, the number of sounding points must be determined in the *CR1Dinv* window. To enter the new sounding data, one selects a "new data" item from the "File". The *SondagePoint* window (Fig. 4) then appears, and allows the user to enter the position of the electrodes. At the bottom of this window, there is a select field in which the number of frequencies is entered. We point out that the number of frequencies is constant,

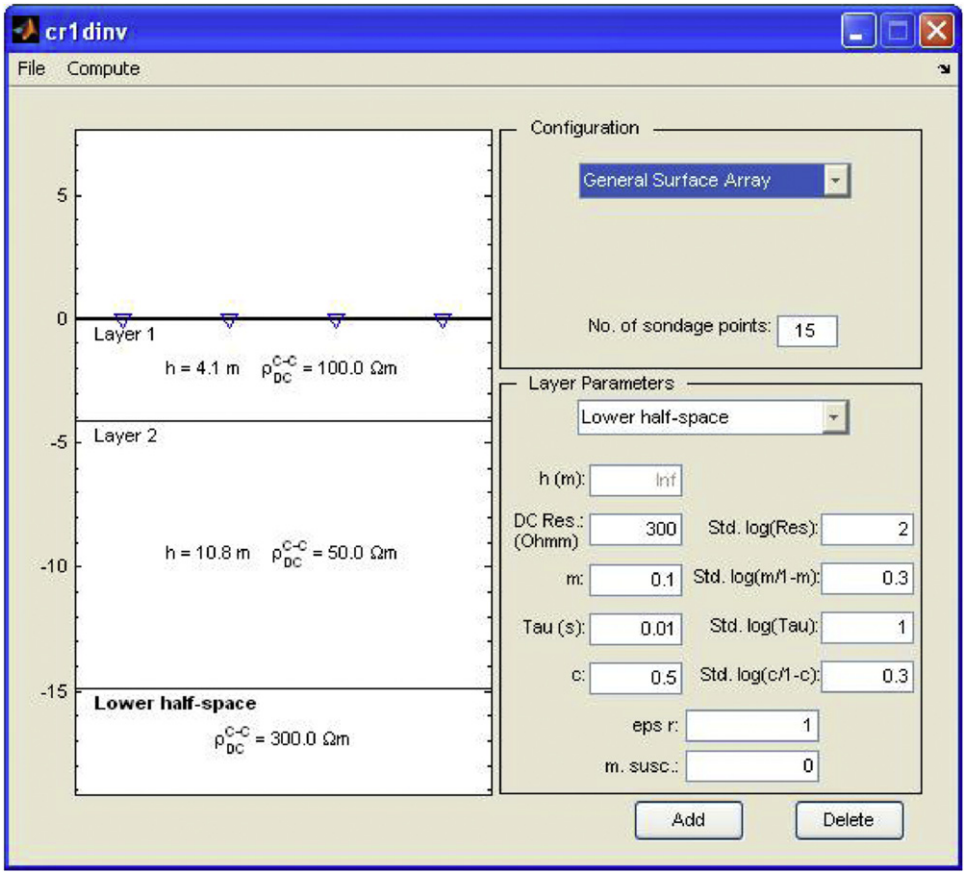

Fig. 3. *CR1Dinv* window: a graphical representation of the model, in which the user can add or delete layers and move boundaries. Right-hand side of the window enables the configuration, model's *a priori* layer parameters, and model's layer parameter standard deviations, to be controlled.

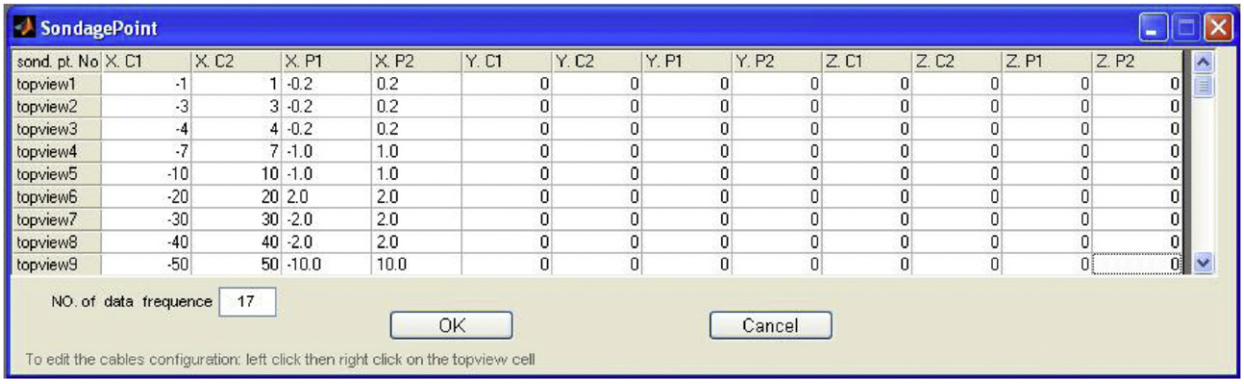

Fig. 4. *SondagePoint* window of *CR1Dinv* features a spreadsheet which allows the electrode coordinates to be entered. A left click, followed by a right click of the mouse gives access to *topview* windows, where the cable configuration of each sounding point can be edited.

for all of the sounding points. Therefore, before clicking on the *topview* button, the number of measured frequencies must be selected. There is a column of *topview* buttons on the left-hand side of the *SondagePoint* window. By left and then right clicking the mouse on the *topview* buttons, a special window is called up, which allows the user to place the electrodes, either by dragging them with the mouse, or by entering new coordinates in the input fields. The *topview* windows also allow the user to add or move segments of the receiver and transmitter wires. Thus, the

influence of the routing of the wires can be taken into account in the frequency domain responses. In the right hand of this window, an Excel spread sheet is provided, which allows the user to enter the data spectrum (frequency in Hertz, amplitude in Ohm.meter, negative phase in milliradians, amplitude error in percent, and phase error in milliradians).

In the *Calculate* window (Fig. 5), the parameters specific to the type of calculation can be adjusted before calling the forward modeling routine (Ingeman-Nielsen and Baumgartner, 2006), as well as the specific inversion routines. For configurations allowing a choice (array configuration), the frequency domain calculation is selected as well as the "full" or "quasi-static" modes. In full mode, *CR1Dinv* selects either the full solution or the non-magnetic first layer solution, depending on the magnetic susceptibility specified for the first layer. In quasi-static mode, the program assumes both non-magnetic and quasi-static approximations, regardless of the values of specified susceptibility and permittivity (Ingeman-Nielsen and Baumgartner, 2006). The forward modeling and inversion routines, which calculate the frequency domain response of the grounded wire configurations and inverse problem, are solved, respectively, in *emgsafwd.m* and *Inversion.m*.

The different parameters used in the inversion part of the *Calculate* window are listed in the following:

- The homotopy coefficient determines the maximum number of divisions along the λ-direction. λ is the homotopy parameter, which varies between 0 and 1.
- The improvement in RMS error is used as a criterion for termination of the routine, at each homotopy inversion step.
- The Gauss–Newton and quasi-Newton options can be used for minimization of the misfit function, at each step of the homotopy inversion.
- The iteration adjustment value is the same as the *ad hoc* parameter ε (real, positive), described in Section 5.

After the calculations have ended, the results are saved into a binary Matlab file along with the model, configuration, and inversed parameters.

Finally, the calculated responses are plotted on the screen as Nyquist diagrams. For each layer, the plots display the convergence processes for each of the parameters.

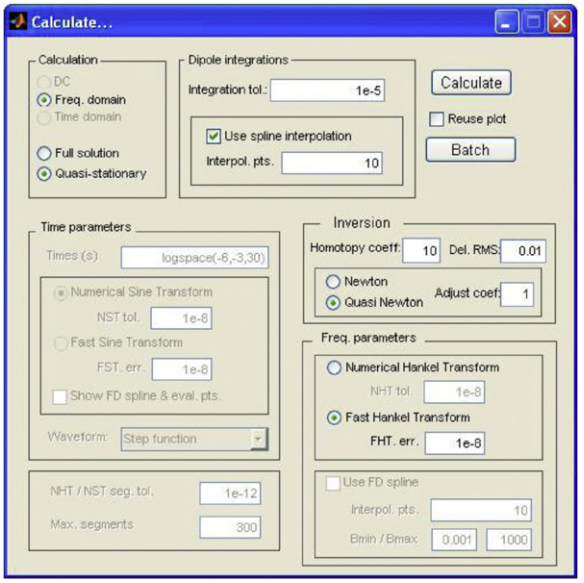

Fig. 5. *Calculate* window of *CR1Dinv* gives the user control over specific parameters of forward modeling (i.e., calculation domain, transform types, tolerances and spline interpolations) and inversion routines (i.e., homotopy coefficient, *ad hoc* value).

8. Results

The results obtained with the inversion method, from two synthetic examples, are presented. The minimum configuration requirement is a Matlab environment, version 7.0.4 (R14). For both examples, we used 17 frequencies in the range between 0.183 Hz and 12 kHz, with logarithmic steps of $12\,\text{kHz}/2^N$, where N is the number of frequencies used in the SIP FUCHS-II equipment.[1]

The first example consists of a half-space Earth. Table 1 describes the initial model, the true and the inversion values of the parameters. The amplitude and phase values are calculated for five different spacings of a dipole–dipole array, at a sounding point. The length of the array line was $\text{AB} = \text{MN} = 50\,\text{m}$ and n, the dipole–dipole separation, changes from 1 to 5. The transmitter and receiver cables

Table 1
Inversed parameters obtained with inversion algorithm, for synthetic spectral induced polarization data, from a half-space Earth.

	Layers	Parameters				*a priori* STD of				Computed STD of				RMS error (%)
		ρ_0 (Ω m)	m	c	τ (s)	$\hat{\rho}_0$	$\hat{m}$	$\hat{c}$	$\hat{\tau}$	ρ_0	m	c	τ	
Initial values		100	0.49	0.1	10									
Real values	1	50	0.8	0.3	10^{-1}	1	0.3	0.3	0.5	230	0.17	0.06	11.5	0.3
Inverted values		49.98	0.7998	0.300	0.0998									

Real values and initial model parameters are shown. Standard deviation (STD) of parameters ρ_0, m, c, and τ are calculated by Jacobian transformation: ($\sigma_{\mathbf{P}} = |\partial\mathbf{P}/\partial\hat{\mathbf{P}}|\sigma_{\hat{\mathbf{P}}}$), where $\sigma_{\mathbf{P}}$ and $\sigma_{\hat{\mathbf{P}}}$ are standard deviations of parameters $\mathbf{P}$ and $\hat{\mathbf{P}}$, respectively.

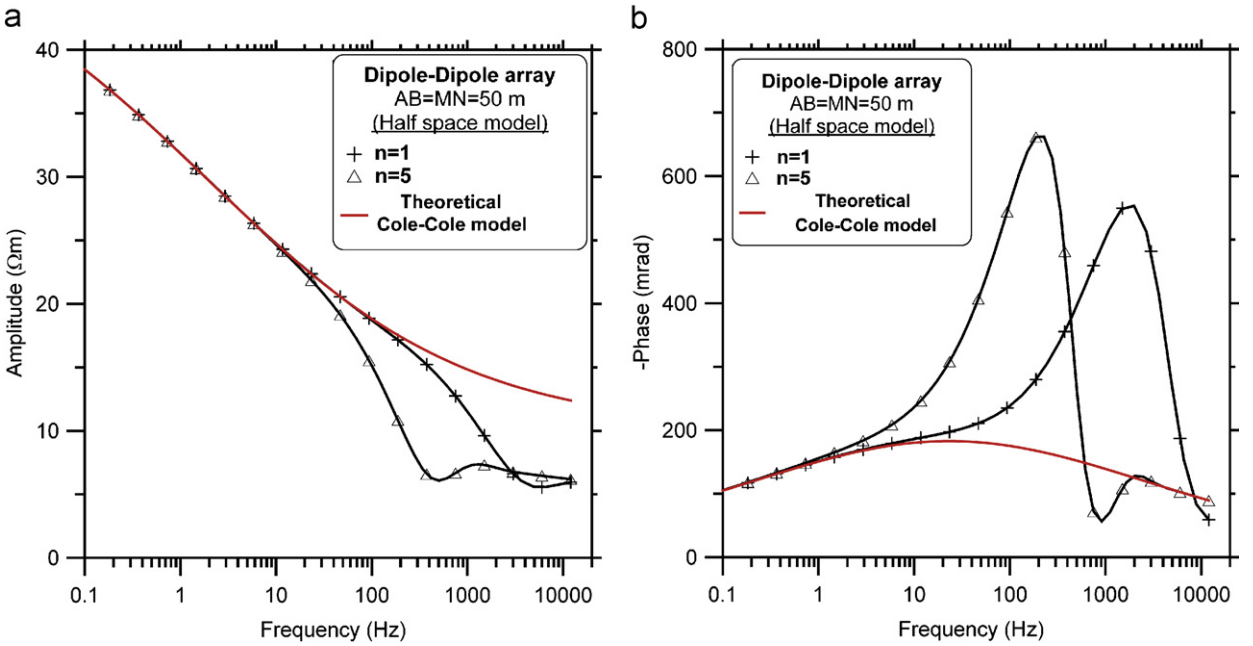

Fig. 6. Amplitude (a) and phase angle (b) vs. frequency, for synthetic example 1 (one layer). A dipole–dipole array is used with AB = MN = 50 m. Dipole–dipole separations of $n = 1$ and $n = 5$ are illustrated, with respect to the theoretical response of the half-space material (red line).

are collinear, with 50 m dipoles. The recovered parameters agree well with the true values. The number of sections in the λ-direction is 10 ($\Delta\lambda = 0.1$). The root mean square error (RMS) obtained is 0.3%. Fig. 6a and b show the amplitude and phase angle vs. frequency, for dipole–dipole separations of $n = 1$ and $n = 5$ respectively, with respect to the theoretical response of the half-space material. It can be clearly seen in Fig. 6 that the EM coupling effects increase with dipole separation.

We used an inversion process for the different starting parameter vectors, and traced path-tracking curves (the curve obtained by plotting the parameters vs. λ, where $\mathbf{h}(\mathbf{P}, \lambda) = 0$ in Eq. (11)). The results show that all path-tracking curves converge to the true value (Fig. 7), even when various chargeability values are used in the starting model (i.e., with m equal to either 0.01, 0.49 or 0.99).

The second synthetic test was based on a two horizontal layer model, with a 10 m thickness for the upper layer. Table 2 shows the starting model, true parameters, and inverted parameters. The recovered electrical parameters agree well with the true values. The amplitude and phase values are calculated for five dipole–dipole array separations, AB = MN = 10 m, and $n = 1$–5. The transmitter and receiver cable lengths were 10 m for both cables. 10% errors are considered for both the amplitude and phase. Fig. 8 shows the Nyquist diagrams for the input data, and for calculated data from the inverted model. The final RMS misfit error is 0.6%.

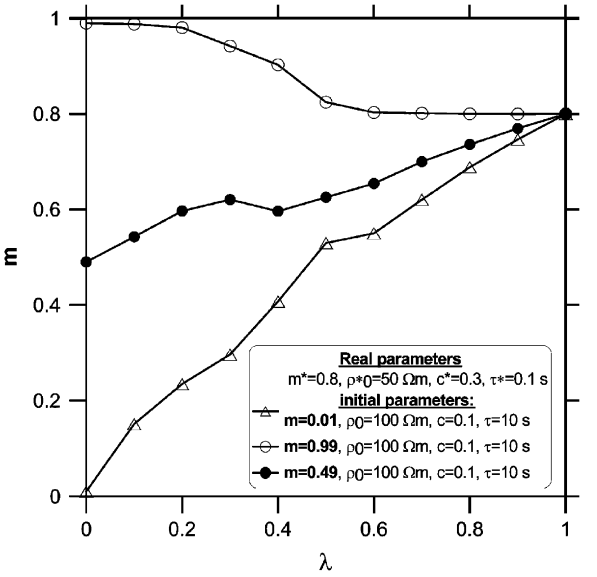

Fig. 7. Homotopy path-tracking curves of the Cole–Cole chargeability parameter, on a half-space Earth with complex resistivity for synthetic example 1. Homotopy parameter lag, $\Delta\lambda = 0.1$, is constant. Different chargeability values are used as starting parameters for the model.

These diagrams show that the EM coupling effects increase with dipole–dipole separation (increase in the imaginary part of the resistivity at higher frequencies, or on the left-hand side of the Nyquist diagrams). As was mentioned in Section 6 (Inversion process), although the user enters the parameters ρ_{0i}, m_i, c_i, τ_i, and h_i, where i is

[1] Radic Research, Complex electrical resistivity field measuring equipment SIP-FUCHS-II: http://www.radic-research.de/Flyer_SIP-Fuchs_II_151104.pdf.

Table 2
Inversed parameters obtained with inversion algorithm, for synthetic spectral induced polarization data, from a half-space Earth containing two layers.

	Layers	Parameters					*a priori* STD of					Computed STD of					RMS error (%)
		ρ_0 (Ω m)	m	c	τ (s)	h (m)	$\hat{\rho}_0$	$\hat{m}$	$\hat{c}$	$\hat{\tau}$	$\hat{h}_i$,	ρ_0	m	c	τ	h	
Initial values		*100*	*0.45*	*0.45*	*0.1*	*2.0*											
Real values	1	50	0.2	0.5	0.1	10	1	0.3	0.3	1	0.1	230	0.17	0.17	0.12	0.46	0.6
Inverted values		49.7	0.195	0.497	0.10	9.94											
Initial values		*1000*	*0.45*	*0.45*	*0.1*	–											
Real values	2	300	0.6	0.5	0.001	–	1	0.3	0.3	0.5	–	2302	0.17	0.17	0.12	–	0.6
Inverted values		304	0.62	0.46	0.0012	–											

Real values and initial model parameters are shown. Standard deviation (STD) of parameters ρ_0, m, c, and τ are calculated by Jacobian transformation: ($\sigma_{\mathbf{P}} = |\partial\mathbf{P}/\partial\hat{\mathbf{P}}|\sigma_{\hat{\mathbf{P}}}$), where $\sigma_{\mathbf{P}}$ and $\sigma_{\hat{\mathbf{P}}}$ are standard deviations of parameters $\mathbf{P}$ and $\hat{\mathbf{P}}$, respectively.

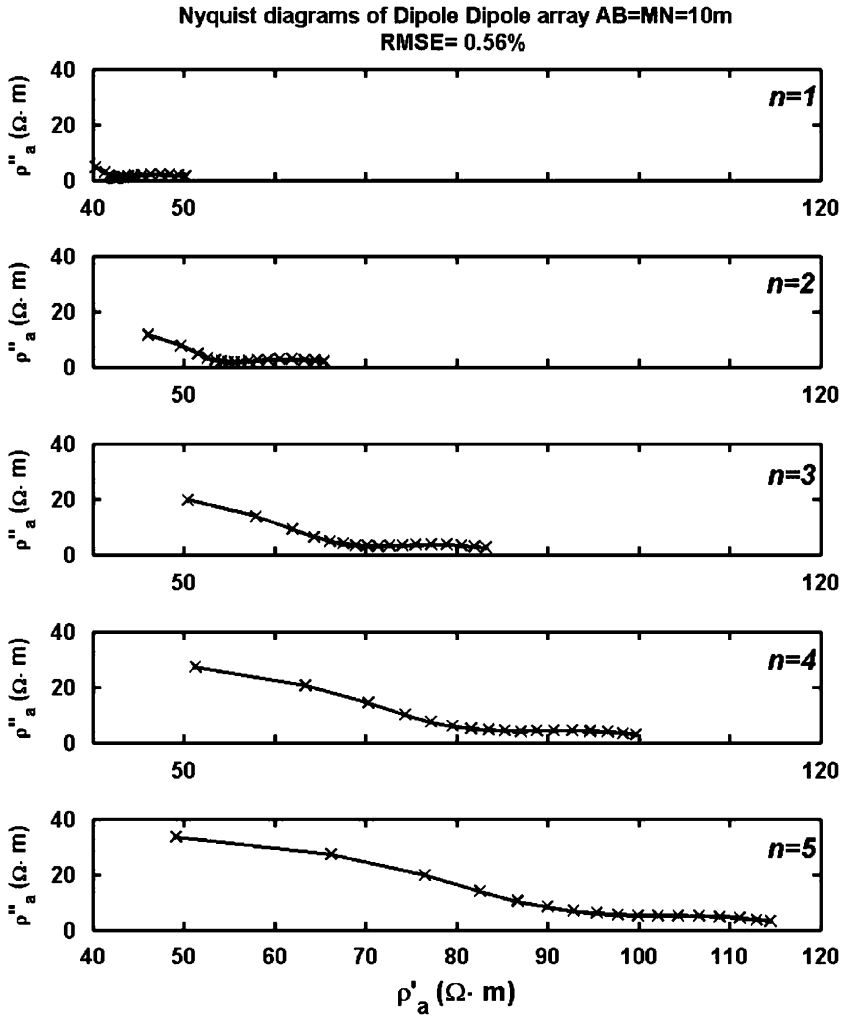

Fig. 8. Nyquist diagrams of data (points) and inversed model (line), for two-layer synthetic example. Frequency varies between 0.183 Hz and 12 kHz. A dipole–dipole array is used with AB = MN = 10 m, and five dipole–dipole separations are used with n = 1–5.

the layer index, the working parameters during inversion process are $\hat{\rho}_{0i}$, $\hat{m}_i$, $\hat{c}_i$, $\hat{\tau}_i$, and $\hat{h}_i$, with symmetric Gaussian distributions. For simplicity, user-entered standard deviations apply for the new parameters. However, it is still possible to derive standard deviations for the parameters ρ_{0i}, m_i, c_i, τ_i, and h_i , by using the Jacobian transformation

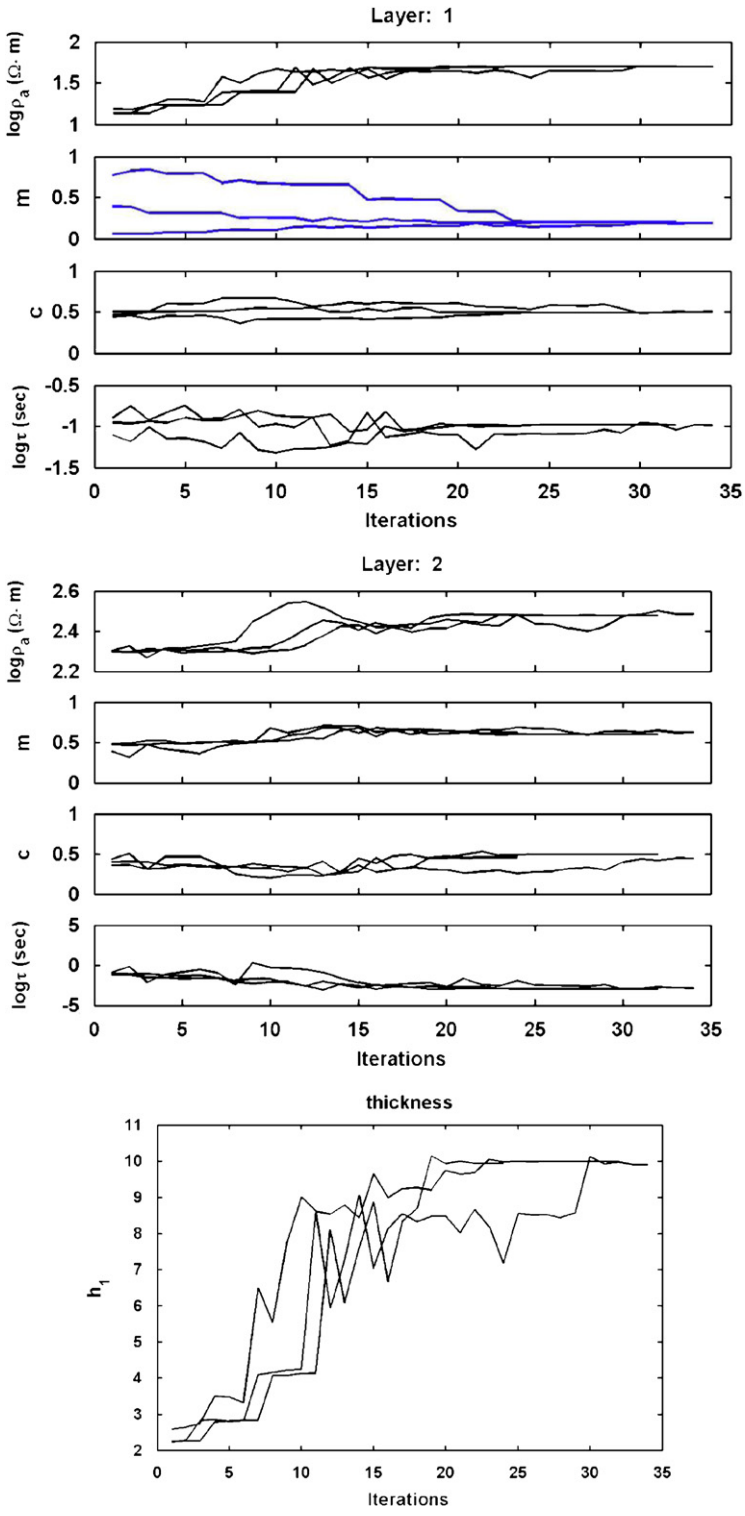

Fig. 9. Homotopy path-tracking of the Cole–Cole parameters for two-layer synthetic example, shown for different iterations. Seven homotopy steps were used. Inversion process is executed for different starting model values of chargeability for the first layer ($m = 0.05$, 0.45, and 0.9, blue curves).

($\sigma_{\mathbf{P}} = |\partial\mathbf{P}/\partial\hat{\mathbf{P}}|\sigma_{\hat{\mathbf{P}}}$), where $\sigma_{\mathbf{P}}$ and $\sigma_{\hat{\mathbf{P}}}$ are the standard deviations for the parameter vectors $\mathbf{P}$ and $\hat{\mathbf{P}}$, respectively. For example, the standard deviation of the Cole–Cole chargeability, m_i, can be calculated from the standard deviation of $\hat{m}_i$, using the relation $\sigma_m = |\partial m/\partial\hat{m}|\sigma_{\hat{m}} = \log(10)[m(1-m)]*\sigma_{\hat{m}}$. The parameters and their standard

deviation are shown in Tables 1 and 2, for each of the synthetic examples. The other conditions selected in the second example were as follows: the homotopy inversion was performed in 7 steps, and the quasi-Newton procedure was used for misfit minimization. Fig. 9 shows the homotopy path-tracking of the Cole–Cole parameters during the course of the successive iterations. Parameter convergence is achieved, whatever value is taken for the chargeability of the initial model (m equal to 0.05, 0.45 or 0.9).

9. Conclusion

A homotopy inversion method is proposed for SIP data, using the Cole–Cole model, based on EM formulation of a 1D Earth. This method further widens the domain of convergence of traditional methods. With this approach, path-tracing is based on a set of predictor–corrector steps, which are obtained by varying the model vector $(\mathbf{P},\lambda)$ by an isometric increment $\Delta\lambda$, in the λ-direction. Local Gauss–Newton and/or quasi-Newton inversion methods are used for the corrector steps. An approximate inversion of the DC resistivity model is first carried out, in order to construct the initial resistivity and thickness models, and is then used as the starting model in the final inversion.

This algorithm has given satisfactory results in tests with data from synthetic models. The results of field data inversion will be presented in a future paper.

Acknowledgement

We are indebted to the ANR-CNRS-INSU-ECCO program (project Polaris II, 2005–2008) in France for their support of this work. We also thank the Referees and the Editor for their useful comments.

Appendix A. Supporting Information

Supplementary data associated with this article can be found in the online version at doi:10.1016/j.cageo.2008.06.001.

References

Abdel Aal, G.Z., Slater, L.D., Atekwana, E.A., 2006. Induced-polarization measurements on unconsolidated sediments from a site of active hydrocarbon biodegradation. Geophysics 71, H13–H24.

Bao, G., Liu, J., 2003. Numerical solution of inverse scattering problems with multi-experimental limited aperture. SIAM Journal on Scientific Computing 25, 1102–1117.

Benavides, A., Everett, M.E., 2007. Non-linear inversion of controlled source multi-receiver electromagnetic induction data for unexploded ordnance using a continuation method. Journal of Applied Geophysics 61, 243–253.

Binley, A., Slater, L., Fukes, M., Cassiani, G., 2005. The relationship between spectral induced polarization and hydraulic properties of saturated and unsaturated sandstone. Water Resources Research 41, W12417.

Brown, R.J., 1985. EM coupling in multifrequency IP and a generalization of the Cole–Cole impedance model. Geophysical Prospecting 33, 282–302.

Cao, Z., Chang, Y., Luo, Y., 2005. Inversion study of spectral induced polarization based on improved genetic algorithm. In: Proceedings Progress In Electromagnetics Research Symposium. Hangzhou, China, pp. 1–5.

Coggon, J.H., 1984. New three-point formulas for inductive coupling removal in induced polarization. Geophysics 49, 307–309.

Cole, K.S., Cole, R.H., 1941. Dispersion and absorption in dielectrics, I. Alternating current fields. Journal of Chemical Physics 9, 341–353.

Dey, A., Morrison, H.F., 1973. EM coupling in frequency and time-domain induced-polarization surveys over a multilayered Earth. Geophysics 38, 380–405.

Dias, C.A., 2000. Developments in a model to describe low-frequency electrical polarization of rocks. Geophysics 65, 437–451.

Everett, M.E., 1996. Homotopy, polynomial equations, gross boundary data, and small Helmholtz systems. Journal of Computational Physics 124, 431–441.

Gasperikova, E., Morrison, H.F., 2001. Mapping of induced polarization using natural fields. Geophysics 66, 137–147.

Ghorbani, A., Camerlynck, C., Florsch, N., Cosenza, P., Revil, A., 2007. Bayesian inference of the Cole–Cole parameters from time and frequency domain induced polarization. Geophysical Prospecting 55, 589–605.

Han, B., Fu, H.S., Li, Z., 2005. A homotopy method for the inversion of a two-dimensional acoustic wave equation. Inverse Problems in Science and Engineering 13, 411–431.

Han, B., Fu, H., Liu, H., 2007. A homotopy method for well–log constraint waveform inversion. Geophysics 72, R1–R7.

Hohmann, G.W., 1973. Electromagnetic coupling between grounded wires at the surface of a two-layer earth. Geophysics 38, 854–863.

Ingeman-Nielsen, T., Baumgartner, F., 2006. CR1Dmod: a Matlab program to model 1D complex resistivity effects in electrical and EM surveys. Computers & Geosciences 32, 1411–1419.

Jegen, M.D., Everett, M.E., Schultz, A., 2001. Using homotopy to invert geophysical data. Geophysics 66, 1749–1760.

Katsube, T.J., Collett, L.S., 1973. Electrical characteristic differentiation of sulphide minerals by laboratory techniques. Geophysics 38, 1207.

Keller, H.B., Perozzi, D.J., 1983. Fast seismic ray tracing. SIAM Journal on Applied Mathematics 43, 981–992.

Kemna, A., 2000. Tomographic inversion of complex resistivity-theory and application. Ph.D Dissertation, University of Bochum, Germany.

Kemna, A., Räkers, E., Dresen, L., 1999. Field application of complex resistivity tomography. In: Proceedings of the 69th Annual International Meeting, Society of Exploration Geophysics, Expanded Abstracts, pp. 331–334.

Kemna, A., Binley, A., Slater, L., 2004. Crosshole IP imaging for engineering and environmental applications. Geophysics 69, 97–107.

Klein, J.D., Sill, W.R., 1982. Electrical properties of artificial clay-bearing sandstone. Geophysics 47, 1593–1605.

Loke, M.H., Dahlin, T., 2002. A comparison of the Gauss–Newton and quasi-Newton methods in resistivity imaging inversion. Journal of Applied Geophysics 49, 149–162.

Loke, M.H., Chambers, J.E., Ogilvy, R.D., 2006. Inversion of 2D spectral induced polarization imaging data. Geophysical Prospecting 54, 287–301.

Luo, Y., Zhang, G., 1998. Theory and application of spectral induced polarization. Geophysical Monograph Series (8), Society of Exploration Geophysicists, Tulsa, p. 171.

Marshall, D.J., Madden, T.R., 1959. Induced polarization, a study of its causes. Geophysics 24, 790–816.

Millett, F.B., 1967. Electromagnetic coupling of collinear dipoles on a uniform half-space. In: Mining Geophysics, Vol. II, Society of Exploration Geophysicists, Tulsa, pp. 401–419.

Mosegaard, K., Tarantola, A., 2002. Probabilistic approach to inverse problems. In: International Handbook of Earthquake and Engineering Seismology (Part A). Academic Press, New York, pp. 237–265.

Pelton, S.H., Ward, S.H., Hallof, P.G., Sill, W.R., Nelson, P.H., 1978. Mineral discrimination and removal of inductive coupling with multifrequency IP. Geophysics 43, 588–609.

Routh, P.S., Oldenburg, D.W., 2001. EM coupling in frequency-domain induced polarization data: a method for removal. Geophysical Journal International 145, 59–76.

Song, L., 1984. A new IP decoupling scheme. Exploration Geophysics 15, 99–112.

Sunde, E.D., 1968. Earth Conduction Effects in Transmission Systems. Dover, New York, p. 370.

Tarantola, A., Valette, B., 1982a. Inverse problems—quest for information. Journal of Geophysics 50, 159–170.

Tarantola, A., Valette, B., 1982b. Generalized non linear inverse problem solved using the least square criterion. Reviews of Geophysics and Space Physics 20, 219–232.

Van Voorhis, G.D., Nelson, P.H., Drake, T.L., 1973. Complex resistivity spectra of porphyry cooper mineralization. Geophysics 38, 49–60.

Vanhala, H., 1997. Mapping oil-contaminated sand and till with the spectral induced polarization (SIP) method. Geophysical Prospecting 45, 303–326.

Vasco, D.W., 1994. Singularity and branching: a path-following formalism for geophysical inverse problems. Geophysical Journal International 119, 809–830.
Vasco, D.W., 1998. Regularization and trade-off associated with nonlinear geophysical inverse problems: penalty homotopies. Inverse Problems 14, 1033–1052.
Vinegar, H.J., Waxman, M.H., 1984. Induced polarization of Shaly sands. Geophysics 49, 1267–1287.
Wait, J.R., Gruszka, T.P., 1986. On electromagnetic coupling removal from induced polarization surveys. Geoexploration 24, 21–27.
Watson, L.T., 1989. Globally convergent homotopy methods: a tutorial. Applied Mathematics and Computation 31, 369–396.
Wynn, J.C., Zonge, K.L., 1975. EM coupling, its intrinsic value, its removal and the cultural coupling problem. Geophysics 40, 831–850.
Wynn, J.C., Zonge, K.L., 1977. Electromagnetic coupling. Geophysical prospecting 25, 29–51.